PHYSICAL REVIEW B **77**, 125317 (2008)

# Determination of the valence band offset of MOVPE-grown $In_{0.48}Ga_{0.52}P$/GaAs multiple quantum wells by admittance spectroscopy

Carlo Ghezzi, Renato Magnanini, Antonella Parisini, and Luciano Tarricone
*CNISM-Dipartimento di Fisica, Università di Parma, Viale Giampaolo Usberti, 7/A, 43100 Parma, Italy*

Enos Gombia
*CNR-IMEM, Parco Area delle Scienze 37/A, 43010 Località Fontanini-Parma, Italy*

Massimo Longo*
*CNR-INFM, Dipartimento di Fisica, Università di Parma, Viale Giampaolo Usberti, 7/A, 43100 Parma, Italy*
(Received 15 November 2007; published 14 March 2008)

The valence band discontinuity of the lattice matched $In_{0.48}Ga_{0.52}P$/GaAs heterostructure was determined through a careful analysis of the temperature and frequency dependence of the admittance of $p^+$/MQW/$n^+$ structures, formed by a nominally undoped InGaP/GaAs multiple quantum well region, interposed between $p^+$ and $n^+$ GaAs layers. The heterostructures were grown through metal organic vapor phase epitaxy by using tertiary butyl arsine and tertiary butyl phosphine as alternative precursors for the V-group elements. The growth conditions were optimized for obtaining sharp interfaces and negligible ordering effects in the cation sublattice. Accounting for the temperature dependence of the Fermi energy and the calculated confining energy (10 meV) of the heavy holes in the wells, a valence band offset $\Delta E_V=(356\pm 5)$ meV was derived from the temperature variation of the resonance frequency at which the isothermal conductance over frequency $G(\omega)/\omega$ curves show a maximum. The experimental uncertainty of this result is significantly low if compared with the wide range (240–400 meV) of the previously reported $\Delta E_V$ values. By considering the band gap difference between InGaP and GaAs, a conduction band offset $\Delta E_C=119$ meV was estimated. The accuracy of the experimental procedure and the reliability of the main assumptions of the admittance spectroscopy measurements were accurately checked. The obtained results were discussed in light of the large and growing amount of literature data by taking into account the influence of the growth conditions on the physical properties of the InGaP/GaAs quantum wells.

DOI: 10.1103/PhysRevB.77.125317 PACS number(s): 73.40.Kp, 73.21.Fg, 73.61.Ey

## I. INTRODUCTION

It has been widely recognized that InGaP lattice matched to GaAs appears as a real alternative to the AlGaAs/GaAs system for the fabrication of Al-free high quality and high reliability devices.[1] This is mainly due to (i) low reactivity to oxygen, (ii) low surface recombination rate, (iii) low propagation velocity of dislocations, (iii) availability of selective etching techniques, and (iv) a minor effect of deep level centers and negligible DX center related effects.

The high direct band gap value and the low effect of deep levels, such as oxygen-related nonradiative recombination centers, favor the fabrication of high performance optoelectronic devices, such as lasers[2,3] and photonic devices.[4] A particular interest has also been devoted to photovoltaic device systems for spatial applications, because of a superior radiation resistance of InGaP in comparison to more usual Si or GaAs based devices.[5–9] The low density of donor related deep traps is an additional advantage in favor of the replacement of AlGaAs with InGaP, also in high electron mobility transistors[10] and heterostructure insulated gate field effect transistors[11] in high-speed circuit applications. Moreover, the InGaP/GaAs heterojunction, which is undoubtedly characterized by a higher valence band offset, is particularly attractive for limiting the minority carrier base-emitter current in heterojunction bipolar transistors (HBT) where InGaP is the emitter. By taking advantage of this property, promising power amplifiers for microwave applications[12,13] and, more recently, quantum well base HBT lasers[14] have been fabricated.

The conduction and valence band offsets $\Delta E_C$ and $\Delta E_V$ at the interface play a major role on the physical properties of a heterojunction and heavily influence the modeling and the performance of any related devices. Consequently, a detailed knowledge of the energy band alignment is highly desirable. In spite of that, the measured band discontinuities at the InGaP/GaAs interface spread over a wide range of data, with experimental uncertainties ranging from 5% up to 30% or more. In particular, against a direct band gap difference lower than 500 meV, experimental values of $\Delta E_V$ and $\Delta E_C$ ranging from 240 to 400 meV (see Table I and Refs. 15–23) and from 30 to 220 meV (see Table II and Refs. 15, 18, and 21–31), respectively, have been reported.

Such a wide spread of data is often ascribed to different growth methods and growth conditions or different measurement techniques. More specifically, the difficult control of the InGaP composition required for the lattice matching to GaAs (that is, $Ga_{0.51}In_{0.49}P$), intermixing effects at the interface, and uncontrolled formation of ordered domains in the cation sublattice are expected to play a major role in affecting the band offsets. To this latter point, it is worth mentioning that ordering can influence the physical properties of the alloy to such an extent that it can be exploited in tailoring the band alignment.[32]

 ©2008 The American Physical Society

TABLE I. Valence band values reported in the literature for the InGaP/GaAs heterostructure. The method of sample growth and the technique of measurement or calculation are also reported.

| $\Delta E_V$ (meV) | Growth technology | Experimental technique or theory | Ref. |
|---|---|---|---|
| $400 \pm 20$ | MBE | Photoluminescence under high pressure | 15 |
| 380 | ALMBE | Pressure dependence and time resolved photoluminescence | 20 |
| 370 | Theory | First-principles pseudopotential: GaAs/InGaP, fully disordered | 21 |
| $356 \pm 5$ | MOVPE | Admittance spectroscopy | This work |
| $330 \pm 20$ | MOMBE | Photoluminescence under high pressure | 17 |
| 320 | MOMBE | Photoreflectance | 16 |
| $310 \pm 15$ | MBE | Capacitance-voltage and current-voltage | 18 |
| $300 \pm 50$ | GSMBE | X-ray photoemission spectroscopy | 19 |
| 285 | MOCVD | Deep level transient spectroscopy | 22 |
| 270 | Theory | First-principles pseudopotential GaAs/InGaP, fully ordered | 21 |
| $240 \pm 10$ | MBE | Capacitance-voltage profiling | 23 |

Generally, optical as well electrical methods have been used in the experimental determinations of band offsets. Amongst electrical methods, admittance spectroscopy of multiple quantum wells (MQWs) has been proven to be very accurate.[33–35] Its advantage is that the band offset is derived through a straightforward analysis of the temperature dependence of an easily measurable resonance frequency, rather than through cumbersome simulations of current-voltage or capacitance-voltage curves, as required in other electrical methods. Nevertheless, admittance spectroscopy has not been employed yet, to our knowledge, for the determination of band offsets in the InGaP/GaAs heterostructure.

In this work, an accurate determination of the valence band discontinuity $\Delta E_V$ at the interface of the lattice matched GaAs/InGaP heterostructure was performed by admittance spectroscopy measurements in $p^+$/MQW/$n^+$ structures, containing an undoped GaAs/InGaP MQW structure, interposed between a $n^+$-doped GaAs substrate and a $p^+$-doped GaAs cap layer. The $p^+$/MQW/$n^+$ structures were grown by metal organic vapor phase epitaxy (MOVPE) using all metalorganic precursors for the V-group elements. In order to minimize any possible effect which could influence the spreading of the obtained band discontinuity, the growth conditions were previously optimized to prevent significant ordering effects in the cation sublattice of the InGaP alloy and to obtain a reasonable interface abruptness giving a well defined quantum well (QW) energy band profile. The reliability of the experimental procedure and of the main assumptions of the admittance spectroscopy method were accurately checked. The obtained results were discussed at the light of the structural and optical properties, elsewhere reported,[9,36,37] of the investigated QW structures and in comparison with the literature data.

TABLE II. Conduction band values reported in the literature for the InGaP/GaAs heterostructure. The method of sample growth and the technique of measurement or calculation are also reported.

| $\Delta E_C$ (meV) | Growth technology | Experimental technique or theory | Ref. |
|---|---|---|---|
| 30 | MOCVD | Collector current vs temperature | 26 |
| $40 \pm 60$ | GSMBE | Cross-sectional STM (nm scale) | 28 |
| $60 \pm 20$ | MBE | Photoluminescence under high pressure | 15 |
| 95 | MBE | Capacitance-voltage and current-voltage | 18 |
| 101 | MOCVD | Capacitance-voltage profiling, indium molar fraction of 35% | 29 |
| $108 \pm 6$ | GSMBE | Photocurrent (internal photoemission) | 25 |
| $119 \pm 5$ | MOVPE | Admittance spectroscopy | This work |
| 120 | Theory | First-principles pseudopotential GaAs/InGaP, fully disordered | 21 |
| 130 | Theory | First-principles pseudopotential GaAs/InGaP, fully ordered | 21 |
| 131 | MOCVD | Capacitance-voltage profiling, indium molar fraction of 31% | 29 |
| $170 \pm 16$ | MOCVD | Current-voltage | 30 |
| 190 | MOCVD | Capacitance-voltage profiling | 24 |
| 198 | MOCVD | Deep level transient spectroscopy | 22 |
| $210 \pm 10$ | MBE | Current-voltage and photoemission | 27 |
| $217 \pm 14$ | MOCVD | Current-voltage | 31 |
| $220 \pm 10$ | MBE | Capacitance-voltage profiling | 23 |

## II. EXPERIMENT

Several $p^+$/MQW/$n^+$ structures with a lattice matched and nominally undoped GaAs/InGaP MQW region interposed between a $n^+$ GaAs (001) substrate and a $p^+$ GaAs cap layer (Fig. 1) were grown by low pressure MOVPE, using tertiary butyl arsine (TBAs) and tertiary butyl phosphine (TBP) as V-group elements sources. The growths were performed at 600 °C using palladium purified $H_2$ as a carrier gas in a horizontal MOVPE Aixtron reactor (AIX 200 RD), supplied with a rotating susceptor in order to avoid in-plane

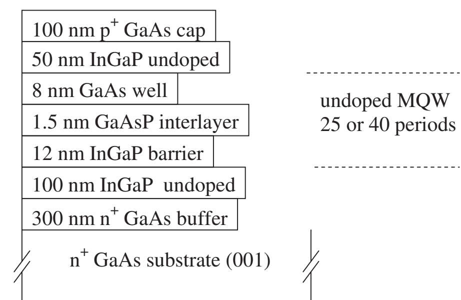


FIG. 1. Sketch of the $n^+$GaAs‖InGaP/GaAs(MQW)‖$p^+$GaAs structures.

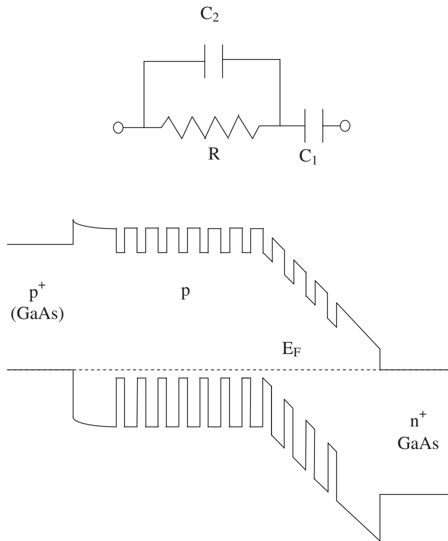


FIG. 2. Equilibrium band bending diagram of the $p^+$/MQW/$n^+$ structure together with the equivalent electrical circuit.

compositional inhomogeneities in the growing sample. The undoped MQW region consisted of 25 to 40 periods of $L_W$ =8 mm GaAs/$L_B$=12 nm InGaP, with the interposition of a 1.5 nm thick GaAsP interlayer at each direct GaAs-on-InGaP interface, to enhance the interface abruptness.[36] Hydrogen-diluted disilane ($Si_2H_6$) was used for the $n^+$ doping of the GaAs buffer layer, whereas the $p^+$ doping of the GaAs cap layer was achieved using dimethylzinc or by taking advantage of the intrinsic doping due to the controlled incorporation of carbon from the methyl radicals.[38] Finally, a few reference samples were grown, where the MQW region was replaced by a single undoped InGaP layer of equal thickness and lattice matched to GaAs. Other details about the growth and the structural and optical properties of the samples are reported elsewhere.[36–39]

In order to perform electrical measurements, an extended AuGeNi Ohmic contact was fabricated on the backside of the $n^+$ GaAs substrate, whereas AuZn dot contacts, 400 $\mu$m in diameter, were deposited on the $p^+$ GaAs cap layer. Finally, a pattern of mesa structures, 6 $\mu$m in depth, was obtained by a 6 min etching in a HCl-$H_2PO_4$-$H_2O_2$ (1-2-1) solution, after deposition of dots of photoresist, 500 $\mu$m in diameter, concentric with the AuZn dots. Admittance measurements were performed in the $10^3$ to $5\times10^6$ Hz frequency range by a HP 4192A impedance analyzer. The amplitude of the sinusoidal test signal was 15 mV.

## III. RESULTS AND DISCUSSION

### A. Equivalent circuit analysis

The equilibrium band bending diagram of the $p^+$/MQW/$n^+$ structure is qualitatively sketched in Fig. 2 together with the equivalent electrical circuit. The MQW region is expected to be only partially depleted near the $n^+$ GaAs contact, since its average electrical conductivity is expected of $p$-type with net acceptor density in the $10^{16}$ cm$^{-3}$

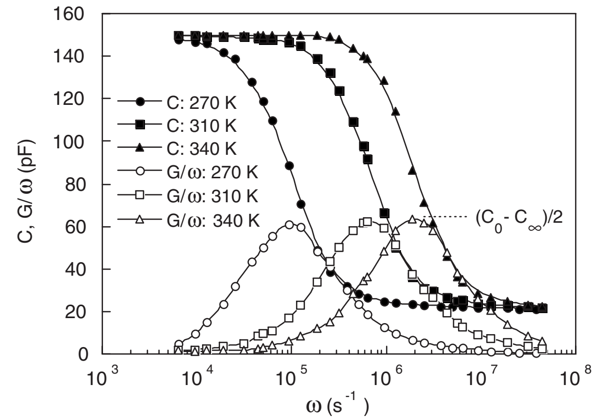


FIG. 3. Typical experimental $C(\omega)$ (full symbols) and $G(\omega)/\omega$ (empty symbols) curves taken at different temperatures in a $p^+$/MQW/$n^+$ structure.

range. In fact, undoped InGaP and GaAs layers grown by the present method resulted in $p$ type with hole density of some $10^{16}$ and $10^{15}$ cm$^{-3}$, respectively. In the equivalent circuit, which is similar to that previously employed for the interpretation of admittance measurements in GaAs/AlGaAs MQW structures,[35] $C_1$ is the capacitance of the depleted MQW region, whereas $R$ and $C_2$ are, respectively, the resistance and the capacitance of the undepleted flatband part of the MQW region. In this way, the measured conductance $G(\omega)$ and capacitance $C(\omega)$ obey the standard equations

$$\frac{G(\omega)}{\omega} = \frac{(\omega/\varpi)[C(0) - C(\infty)]}{1 + (\omega/\varpi)^2},$$

$$C(\omega) = \frac{C(0) - C(\infty)}{1 + (\omega/\varpi)^2} + C(\infty). \quad (1)$$

Here, $\omega=2\pi f$ is the angular frequency of the small amplitude test signal, $C(0)$ and $C(\infty)$ are the measured capacitances in the low and high frequency limits, respectively, related to $C_1$ and $C_2$ by the equations

$$C(0) = C_1, \quad C(\infty) = \frac{C_1C_2}{C_1 + C_2}, \quad (2)$$

and $\varpi$ is the resonance angular frequency given by

$$\varpi = \frac{1}{R(C_1 + C_2)} = \frac{C(0) - C(\infty)}{RC(0)^2}. \quad (3)$$

Examples of experimental $C(\omega)$ and $G(\omega)/\omega$ curves taken at different temperatures are shown in Fig. 3, where the step behavior of $C(\omega)$, with inflection point at $\varpi$, and the peak shape of $G(\omega)/\omega$, with maximum at $\varpi$, are clearly evidenced. The peak value $G(\varpi)/\varpi$, being equal to $[C(0) - C(\infty)]/2$, as expected, is independent of $\varpi$. Moreover, $C(0)$ and $C(\infty)$ are practically independent of temperature so that the observed increase of $\varpi$ with temperature can be directly ascribed to a decrease of the series resistance $R$. As already mentioned, the series resistance $R$ is practically due to the undepleted MQW region, since contributions of contact re-

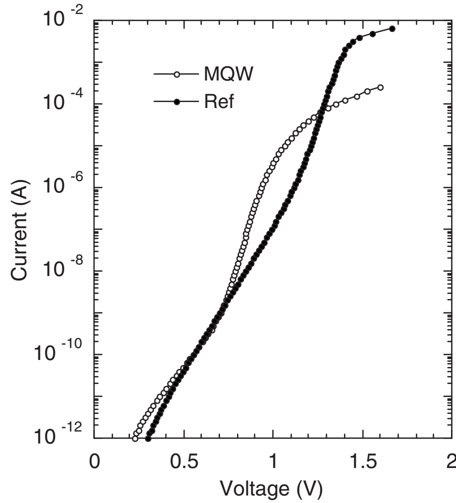


FIG. 4. Comparison of direct current-voltage curves measured at $T=300$ K in a $p^+/\text{MQW}/n^+$ junction (○) and in the corresponding $p^+/\text{InGaP}/n^+$ reference sample (●). In the latter case, the series resistance is about 2 orders of magnitude lower.

sistances are negligible. This point is confirmed by the results of Fig. 4, where the direct current-voltage curve of a $p^+/\text{MQW}/n^+$ junction is compared with the corresponding one of a $p^+/\text{InGaP}/n^+$ reference junction, in which the MQW region is replaced by an undoped InGaP layer of equal thickness. In fact, a simple examination of the figure indicates that, in the latter case, the series resistance is about 2 orders of magnitude smaller than in the MQW case. At a given temperature, $R$ is then proportional to the $L_{\text{und}}$ length of the undepleted MQW region, that is, $L_{\text{und}}=L-S(\varepsilon/C_1)$, where $L$ is the total MQW length and $S(\varepsilon/C_1)=L_{\text{dep}}$ is the thickness of the depleted MQW region ($\varepsilon$ is the mean dielectric constant of the MQW region and $S$ the junction area). Consequently, the resonance frequency becomes

$$\varpi = AF\{C(0),C(\infty)\}$$

with

$$F\{C(0),C(\infty)\} = \frac{C(0)-C(\infty)}{[L-S(\varepsilon/C(0))]C(0)^2}, \tag{4}$$

where $A$ is a constant at a given temperature. The validity of Eq. (4) can be checked by measuring $\varpi$ as a function of the applied reverse bias $V_R$, whose effect is that of varying the $C_1=C(0)$ capacitance. In fact, admittance measurements at $T=340$ K and at different values of $V_R$ exhibit an appreciable increase of $\varpi$ as $V_R$ is increased, as shown in Fig. 5(a). Moreover, $\varpi$ increases linearly with the quantity $F\{C(0),C(\infty)\}$, as shown in Fig. 5(b). Here, in the evaluation of $F$, a mean dielectric constant $\varepsilon=12\varepsilon_0$ is used, whereas $C(0)$ and $C(\infty)$ are the experimental capacitance values of Fig. 5(a). All this corroborates the analysis leading to Eq. (4) and demonstrates that the choice of the equivalent circuit in Fig. 2 is well grounded.

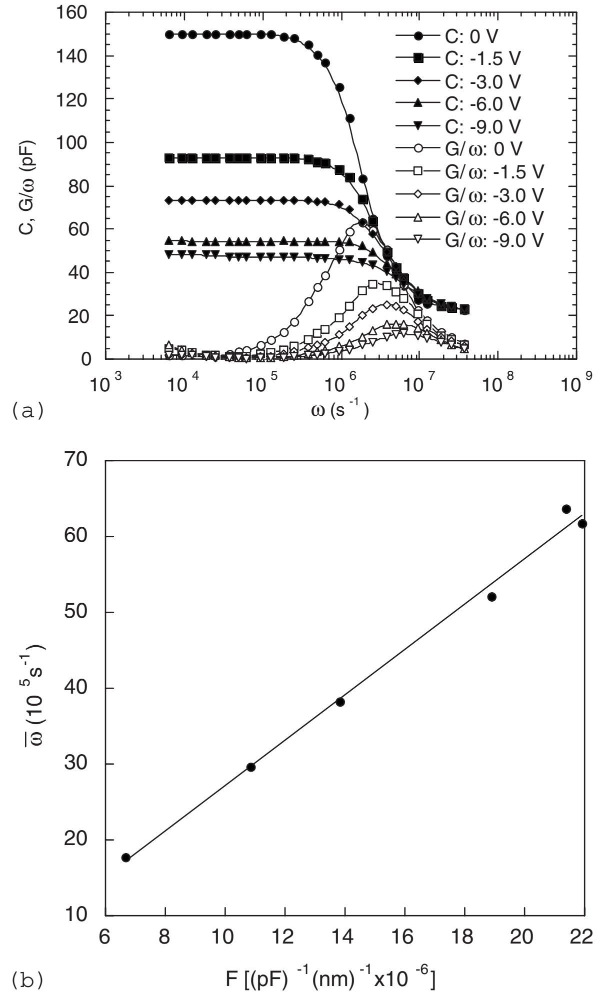


FIG. 5. (a) $C(\omega)$ (full symbols) and $G(\omega)/\omega$ (empty symbols) curves taken at the same temperature of 340 K but with different reverse biases $V_R$. (b) Resonance frequency $\varpi$ as derived by curves of Fig. 5(a) plotted vs the function $F\{C(0),C(\infty)\}$, given by Eq. (4). Here, $C(0)$ and $C(\infty)$ are the experimental capacitances of (a).

At the end of this section, two points deserve a few comments. The first one concerns the analysis of the $C(0)$-$V_R$ plots, since it is known that capacitance-voltage profiles of MQW structures may reveal nonuniform distributions of carriers.[40] In our samples, however, the $C(0)$-$V_R$ profiles revealed apparently uniform distributions of carriers corresponding to net acceptor densities in the range of $(3-6)\times10^{16}\ \text{cm}^{-3}$ (see Fig. 6). This result is consistent with the calculated Debye lengths of 18–26 nm, considerably larger than the barrier thickness of 12 nm in the MQW, so that the apparent carrier distribution becomes flattened, as also demonstrated through simulations under similar conditions.[40]

The second question is on the physical significance of $C(0)$ and $C(\infty)$. As already mentioned, from circuit analysis, we get $C(0)=C_1=S(\varepsilon/L_{dep})$, which is an obvious result since a low frequency variation of the applied voltage can be easily followed by the charge disturbance produced at the edge $L_{dep}$ of the depleted region. On the contrary, a high frequency voltage variation can produce a charge disturbance only at the edges of the whole region of total length $L$ between the

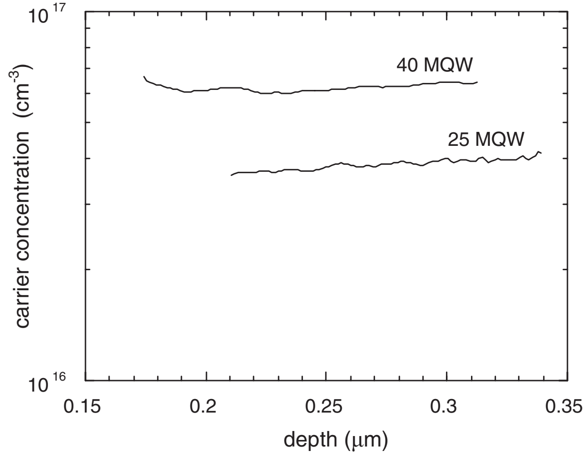


FIG. 6. Carrier profiles obtained by $C(0)$ vs $V_R$ measurements in the $p^+$/MQW/$n^+$ samples with 40 and 25 MQWs.

$n^+$ and $p^+$ contacts, so that we must have $C(\infty)=S(\varepsilon/L)$. This is confirmed by the experimental value $C(\infty)=20$ pF, practically independent of reverse voltage, giving $L=1063$ nm in satisfactory agreement with the expected value of 1010 nm for a 40 period MQW structure. Finally, from Eqs. (2), we get

$$C_2 = \frac{C(0)C(\infty)}{C(0)-C(\infty)} = \frac{S\varepsilon}{L_{und}} \tag{5}$$

for the $C_2$ capacitance of the undepleted MQW region.

### B. Determination of the valence band offset

The temperature dependence of the $R^{-1}$ conductance of the undepleted $p$-type MQW region is found by considering that at high temperatures, the perpendicular conduction is due to thermionic emission of holes over the InGaP barriers. Owing to arguments quite similar to those in Refs. 33 and 34, the thermionic current $J$ can be written as

$$J = q(N_{hh}v_{hh} + N_{lh}v_{lh})\exp\left(-\frac{E_F - E_{VB}}{K_BT}\right)\left[\exp\left(\frac{qV_S}{2K_BT}\right) - 1\right], \tag{6}$$

where the parallel conductions into the heavy (hh) and light (lh) hole valence bands of the barrier material are taken into account. In Eq. (6), $E_F$ is the Fermi energy, $E_{VB}$ the valence band top of the InGaP barrier, $V_S=VL_W/2L$ is the voltage drop on a QW, $V$ is the voltage drop on the undepleted MQW region, and $K_B$ the Boltzmann constant. $N_{hh}$ ($N_{lh}$) is the three-dimensional (3D) density of states and $v_{hh}$ ($v_{lh}$) the thermal velocity in the heavy hole (light hole) InGaP valence band. For small voltages, such as $qV_S \ll K_BT$, Eq. (6) reduces to

$$J = \frac{I}{S} = \alpha T^2 \frac{qV_s}{2K_BT}\exp\left(-\frac{E_F - E_{VB}}{K_BT}\right), \tag{7}$$

where $\alpha$ resumes all the temperature independent preexponential factors of Eq. (6), so that, by taking into account Eq. (3),

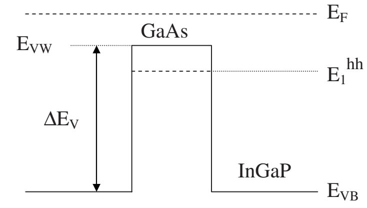


FIG. 7. Energy levels and valence band profile for a QW in the undepleted $p$-type MQW region. $E_F$ is the Fermi energy. $E_{VW}$ and $E_{VB}$ are the valence band top in the GaAs well and in the InGaP barrier, respectively. $E_1^{hh}$ is the deeper energy level for the confined holes.

$$\varpi = \text{const} \times R^{-1}\exp\left(-\frac{E_F - E_{VB}}{K_BT}\right) = BT\exp\left(-\frac{E_F - E_{VB}}{K_BT}\right), \tag{8}$$

where the factor $B$ is independent of temperature. Introducing $E_1^{hh}$ as the lowest energy level for the heavy holes confined in the QW (see Fig. 7), we have $E_F-E_{VB}=(E_F-E_1^{hh})+(E_1^{hh}-E_{VB})$ and consequently

$$\ln\left(\frac{\varpi}{T}\right) = \ln B - \frac{(E_F - E_1^{hh})}{K_BT} - \frac{(E_1^{hh} - E_{VB})}{K_BT}. \tag{9}$$

Owing to this equation, the energy difference $(E_1^{hh}-E_{VB})$ can be obtained by analyzing the temperature dependence of $\ln(\varpi/T)$, if the temperature dependence of the Fermi energy is known. As discussed in the Appendix, a simplified solution of Eq. (9) can be considered if (i) the number of holes confined in the QW does not change appreciably with temperature, (ii) the two-dimensional hole gas is not degenerate, and (iii) only the lowest heavy hole subband is populated. In fact, under these conditions, one gets

$$(E_F - E_1^{hh}) = K_BT\ln(CK_BT), \tag{10}$$

where $C$ is a constant with temperature, so that Eq. (9) takes the following simpler form:

$$\ln\varpi = \ln\left(\frac{B}{CK_B}\right) - \frac{(E_1^{hh} - E_{VB})}{K_BT}, \tag{11}$$

and a simple Arrhenius plot of $\ln\varpi$ vs $(K_BT)^{-1}$ gives $(E_1^{hh}-E_{VB})$. As reported in Ref. 41, this analysis gives $(E_1^{hh}-E_{VB})=(336\pm5)$ meV.

Although the (i) hypothesis may be justified and it can be shown that the (ii) condition is well satisfied in the present cases (see the Appendix), the occupancy of higher hole subbands cannot be completely neglected at the temperatures (250–300 K) of the present experiment (see the Appendix). The above quoted value for $(E_1^{hh}-E_{VB})$ could then be refined by including the contributions of higher subbands in the evaluation of the temperature dependence of the Fermi level. The difference $(E_1^{hh}-E_{VB})$ can be obtained by plotting the more complicated function $Y(T)$ derived from Eq. (9):

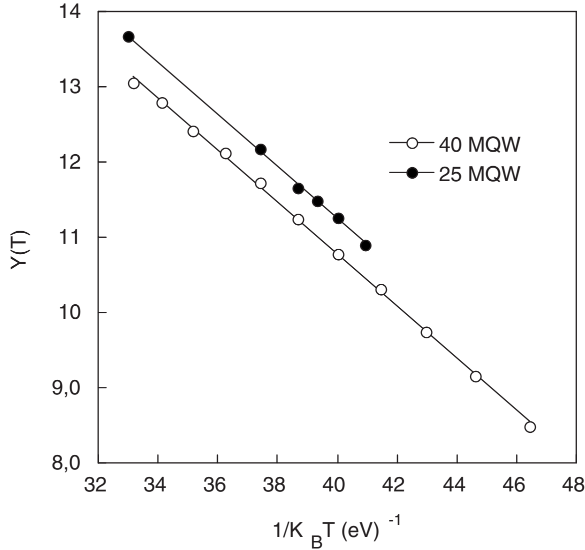


FIG. 8. $Y(T)$ function vs $(K_BT)^{-1}$. Open circles and full dots are data taken in the samples with 40 and 25 MQWs, respectively. The slope gives $(E_1^{hh}-E_{VB})=346\pm5$ meV.

$$Y(T)=\ln\left(\frac{\varpi}{T}\right)+\frac{(E_F-E_1^{hh})}{K_BT}=\ln B-\frac{(E_1^{hh}-E_{VB})}{K_BT} \quad (12)$$

vs $(K_BT)^{-1}$. Figure 8 shows the $Y(T)$ data for both the 40 and 25 period MQWs, taking into account the occupancy of four hole subbands: From the equal slopes of the observed linear behaviors, one gets $(E_1^{hh}-E_{VB})=(346\pm5)$ meV, which is 10 meV higher than the value derived through the assumption of Eq. (10). The inclusion or not of the fourth subband, that is, the $n=3$ heavy hole subband (see the Appendix), resulted in a variation of about 2 meV in the coefficient $(E_1^{hh}-E_{VB})$, smaller than the experimental uncertainty; the effect of higher subbands is therefore expected to be negligible. As concerns the $\ln(B)$ term, the fitting of the $Y(T)$ data gave $24.6\pm0.2$ and $25.2\pm0.4$ for the 40 and 25 period MQW, respectively, resulting therefore in a mean shift between the two intercepts of 0.6. These values can be compared to those calculated by the expression

$$B=\frac{C(0)-C(\infty)}{C(0)^2}\frac{SL_Wq^2}{2L_{und}K_BT^2}(N_{hh}v_{hh}-N_{lh}v_{lh}), \quad (13)$$

which is obtained through Eqs. (6)–(8) and (3). Using $\nu=(K_BT/2\pi m)^{1/2}$ for the thermal velocities ($m$ is the effective hole mass), the calculated $\ln B$ values resulted to 24.8 and 25.5, respectively, in fair agreement with the experimental ones: The small difference in the two values is simply related to the different lengths $L_{und}$ of the undepleted MQW region and to the $C(0)$ and $C(\infty)$ capacitances of the two samples.

Finally, the valence band offset is given by $\Delta E_V=(E_1^{hh}-E_{VB})+(E_{VW}-E_1^{hh})$. Here, $E_{\mathrm{VW}}$ is the top of the GaAs valence band (see Fig. 7) and $(E_{VW}-E_1^{hh})$ is the confinement energy of the heavy holes, which must be calculated for a well depth consistent with the estimated $\Delta E_V$ value. A good agreement is obtained for $(E_{VW}-E_1^{hh})=9.92$ meV (see the Appendix for details), giving $\Delta E_V=(356\pm5)$ meV. In addition, since the difference in band gaps between InGaP and GaAs resulted in $\Delta E_g=475$ meV at the mean temperature ($T_m\sim300$ °K) of the present experiment, a conduction band offset $\Delta E_C=(119\pm5)$ meV may be expected.

### C. Discussion

Wide sets of $\Delta E_V$ and $\Delta E_C$ values obtained in the last 20 years by using several experimental methods in InGaP/GaAs heterostructures, grown by different epitaxial techniques, are given in Tables I and II, respectively. Generally, the growth conditions are expected to significantly influence the formation of the interfaces and, consequently, of the band offset values, although also the experimental methods employed for their evaluation and their accuracy contribute to the scattering of the data. As reported in Table I, the values obtained for $\Delta E_V$ are spread in the rather wide range of 240–400 meV. Our result of $356\pm5$ meV is between the value of 370 meV, calculated through a first-principles pseudopotential approach by Froyen *et al.*[21] for a fully disordered InGaP/GaAs interface, and the one of $330\pm20$ meV, obtained from pressure induced low temperature photoluminescence by Leroux *et al.* in single QW grown by metalorganic molecular beam epitaxy (MOMBE).[17] Moreover, our value is not far from that of 320 meV, determined by G. Arnaud *et al.* through photoreflectance spectroscopy, again on MOMBE grown QWs.[16] Concerning the conduction band offset, the value of $\Delta E_C=(119\pm5)$ meV estimated here falls between the value of $108\pm6$ meV, obtained by Haase *et al.* through internal photoemission measurements on *p-i-n* GaAs/InGaP heterojunctions grown by gas source molecular beam epitaxy (GSMBE),[25] and the value of 120 meV, calculated by Froyen *et al.* for a fully disordered InGaP/GaAs interface.[21]

The good agreement between the values determined here for $\Delta E_V$ and $\Delta E_C$ and those calculated by Froyen *et al.* is probably not fully surprising. In fact, preliminary investigations of the structural and optical properties of the InGaP/GaAs QWs employed here showed a minor or negligible superlattice ordering effect. In particular, a narrow line shape of the band to band recombination emission peak at an energy of 1.998 eV with a full width at half maximum value of about 10 meV was detected at the temperature of 10 K on a 5 $\mu$m thick InGaP layer, grown under similar experimental conditions ($T_g=580$ °C, unpublished data). This result, comparable to the state of the art for the bulklike InGaP/GaAs heterostructure, implies a negligible ordering effect (see Fig. 4 in Ref. 42) and a good control of the residual strain. As a further evidence of this fact, photoluminescence spectra, taken in bulklike nominally undoped InGaP layers grown under similar conditions, showed that the main emission peak due to band to band recombination was free from the anomalous behavior which could be evidenced in the presence of superlattice ordering, or by varying the temperature, or by increasing the laser excitation intensity.[42]

Further reasons which may affect the band offset data are related to the difficult control of the InGaP composition near the value corresponding to the lattice matching to GaAs.

Owing to the sharp variation of the lattice constant of the InP-GaP ternary alloy as a function of the In content, any small deviation from the lattice match induces a shift from compressive to tensile strain conditions. As it has been previously observed, this is the reason of important shifts of the QW photoluminescence lines, ascribed to a modification of the conduction band offset.[43] Moreover, Dong *et al.*[28] reported a remarkable variation of $\Delta E_C$ because of an indium content fluctuation at the InGaP/GaAs interface which has been observed through a cross-sectional scanning-tunneling-microscope (STM) analysis performed at the nanometric scale. Finally, the major role of the fluctuations of the indium content, especially in affecting the conduction band offset, has been confirmed by Park *et al.* through *C-V* profiling of single heterojunctions.[29]

In the present case, the optimization of the MOVPE growth conditions contributed to minimize the indium content fluctuations, as proven by the suppression of an anomalous photoluminescence emission at low energy, ascribed to the formation of an uncontrolled quaternary layer at the interface of the InGaP/GaAs QWs.[36] Moreover, our InGaP/GaAs QWs exhibited excitonic emission peaks whose energies followed the variation of the well width, in agreement with the theory,[36] thus suggesting a good control of the interface abruptness. In addition, the limitation of the residual strain in the InGaP/GaAs heterostructures only allowed us to stack up to 30 periods of 8 nm/12 nm GaAs/InGaP QWs without overcoming the critical thickness for the strain relaxation.[37] As further evidence of the good quality of the MQWs employed here, a fine structure of the confined states was evidenced by photocurrent spectra (see Fig. 5 in Ref. 37) which pointed out, even at room temperature, the splitting of the photocurrent peaks related to the transitions from the $n=1$ heavy or light hole states to the $n=1$ electron state, with energies in excellent agreement with the theory.[37]

Finally, one should also consider that in III-V heterostructures sharing neither common anions nor common cations, two different kinds of interfaces may exist, which are GaP or InGaAs in the present case. This should lead to different interface strains and dipoles and hence, in principle, to different band offsets. Indeed, an *in situ* determination by photoelectron spectroscopy on a similar system, that is, the InP/InGaAs heterostructure grown by MOMBE, has shown an asymmetry of 180 meV in the valence band offset at the direct and inverse interfaces.[44] However, such an asymmetry was ascribed to other causes, which are In segregation and P and As intermixing at the interfaces.[44] To our knowledge, similar *in situ* investigations have not been performed in the InGaP/GaAs heterostructures. However, In segregation and P and As intermixing should be practically suppressed in our heterostructures owing to the employment of optimized gas switching sequences during the growth of the direct and indirect interfaces, clearly described in Ref. 36. As reported in Refs. 45 and 46, such sequences ensure abrupt interfaces and suppress, at both interfaces, the formation of a low-band-gap quaternary layer, which degrades optical and electrical properties of the heterostructures. Although we cannot better specify the stoichiometry of the two interfaces, we remark that in our structures, the observed electronic transitions between quantum states are consistent with the expectation of a model for a rectangular symmetric QW; therefore, we have no reason to hypothesize relevant differences between the barrier heights at the two interfaces. In any case, the value of the valence band offset resulting from our analysis should be understood as averaged on the two interfaces.

## IV. CONCLUSIONS

As proven by the large spread of values reported in the last 20 years, the values of the valence and conduction band discontinuities of the InGaP/GaAs heterostructure are still a matter of discussion in spite of the relevance of this structure in several device applications.

We grew lattice matched InGaP/GaAs MQWs with different number of periods by MOVPE, using TBAs and TBP instead of the common precursors arsine ($AsH_4$) and phosphine ($PH_4$) for the V-group elements. Beyond their lower toxicity, the alternative precursors TBAs and TBP favor a better abruptness of the InGaP/GaAs interface, as it has been previously reported.[47–49] The growth conditions of the QWs were preliminary optimized by limiting the residual strain and avoiding the formation of uncontrolled quaternary layers at the interface, as well as of ordered domains in the cation sublattice. Samples of $p^+$/MQW/$n^+$ structures with the undoped MQW system interposed between $n^+$ and $p^+$ GaAs were then fabricated to perform admittance spectroscopy measurements for an accurate determination of the valence band offset.

The equivalent circuit of the sample and the main assumptions of the admittance spectroscopy method were analyzed in detail in order to check the reliability of the experimental procedure and the final uncertainty of the experimental results. The difference between the lowest energy level for the heavy holes confined in the QW and the InGaP valence band top level $(E_1^{hh}-E_{VB})=(346\pm 5)$ meV was obtained. Then, accounting for the confining energy of the heavy holes (9.9 meV), as calculated by the envelope function approximation for the investigated QWs, a valence band discontinuity $\Delta E_V=356\pm 5$ meV was determined. Considering the well established difference between the InGaP and GaAs band gaps, which results in $\Delta E_g=475$ meV at the mean temperature ($T_m\sim 300$ K) of the present experiment, a conduction band offset $\Delta E_C=(119\pm 5)$ meV was derived.

In conclusion, the admittance spectroscopy method applied to InGaP/GaAs MQW structures, grown under optimized conditions, leads to accurate and reliable values of the band offsets, in good agreement with the calculations previously reported for a fully disordered InGaP/GaAs interface.

## ACKNOWLEDGMENTS

The authors are grateful to R. Jakomin and S. Vantaggio of the Physics Department of the University of Parma for their help in the MOVPE growth and to A. Motta of the IMEM-CNR Institute of Parma for the preparation of ohmic contacts and mesa structures. Many thanks are also due to C. Bocchi, F. Germini, L. Nasi, and L. Lazzarini of the IMEM-

CNR Institute for the structural investigations whose main results are referred to in this paper.

## APPENDIX

It can be easily shown that the sheet hole density $p_s$ in a single QW is related to the Fermi energy by the equation

$$p_S = \frac{K_B T}{\pi\hbar^2}\left\{ m_{hh}\sum_{j=1}^{r} \ln\left[1+\exp\left(-\frac{E_F - E_j^{hh}}{K_B T}\right)\right] + m_{lh}\sum_{j=1}^{s} \ln\left[1+\exp\left(-\frac{E_F - E_j^{lh}}{K_B T}\right)\right]\right\}. \quad (A1)$$

Here $m_{hh}$, $E_j^{hh}$ and $m_{lh}$, $E_j^{lh}$ are the effective masses and the edge energies of the two-dimensional subbands for heavy and light holes, respectively; the sums are extended to the $r$ and $s$ confined states of perpendicular motion. For a nondegenerate gas of heavy holes, so that $(E_F - E_j^{hh}) \gg K_B T$, the heavy hole density $p_S^{hh}$ can be written as

$$p_S^{hh} \cong \frac{K_B T}{\pi\hbar^2}\left\{ m_{hh}\exp\left(-\frac{E_F - E_1^{hh}}{K_B T}\right) \times \left[1+\sum_{j=2}^{r}\exp\left(-\frac{E_1^{hh} - E_j^{hh}}{K_B T}\right)\right]\right\}, \quad (A2)$$

and a quite similar expression applies for the density $p_S^{lh}$ of light holes. If the only relevant contribution to $p_s$ is that of the first heavy hole subband, we have

$$(E_F - E_1^{hh}) \cong K_B T \ln \frac{m_{hh} K_B T}{\pi\hbar^2 p_S}, \quad (A3)$$

which is Eq. (10) with $C = m_{hh}/\pi\hbar^2 p_S$.

The temperature dependence of the Fermi level can be evaluated under the hypothesis that $p_s$ is independent of temperature, which is a reasonable statement considering that practically all the acceptors in the InGaP barrier remain ionized when the temperature is varied. In summary, if we make use of approximation (A3), the energy $(E_1^{hh} - E_{VB})$ can be directly obtained by the Arrhenius plot $\ln \varpi$ vs $(K_B T)^{-1}$, as explained in Sec. III B [see Eq. (11)].

For better refinements, the temperature dependence of $E_F$ can be derived through the general expression (A1) and consequently the energy $(E_1^{hh} - E_{VB})$ should be obtained by following Eq. (12). To perform a more refined analysis, the eigenvalues $(E_{VW} - E_j^{hh})$ and $(E_{VW} - E_j^{lh})$ were then evaluated for an 8 nm wide QW: The standard Schrödinger equation of a particle in a single finite square well (decoupled MQWs) was solved in the limit of $T=0$ K by assuming a well with $\Delta E_V = 356$ meV. The values $\gamma_1 = 6.85$ (4.2) and $\gamma_2 = 2.30$ (1.35) were used for the Luttinger parameters of GaAs (InGaP) to obtain the heavy and light hole effective masses in both materials.[36] Nonparabolicity effects were neglected.

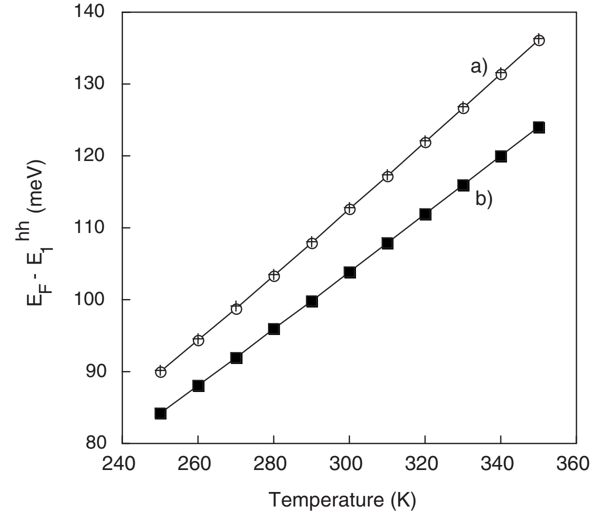


FIG. 9. Temperature dependence of $(E_F - E_1^{hh})$ by considering (a) the occupancy of the first four hole subbands with the Fermi-Dirac statistics (○) or Bolzmann statistics (+) and (b) the occupancy of only the $E_1^{hh}$ subband with Bolzmann statistics. The calculations are performed for $p_s = 1.27 \times 10^{11}$ cm$^{-2}$.

The temperature dependence of the Fermi level was subsequently derived by considering $p_s$ independent of temperature and including in Eq. (A1) the contributions of the first four hole subbands, having edges at the calculated eigenvalues of $(E_{VW} - E_1^{hh}) = 9.925$ meV, $(E_{VW} - E_1^{lh}) = 36.65$ meV, $(E_{VW} - E_2^{hh}) = 39.96$ meV, and $(E_{VW} - E_3^{hh}) = 89.81$ meV. The total hole sheet densities $p_s = 1.27 \times 10^{11}$ cm$^{-2}$ and $p_s = 0.77 \times 10^{11}$ cm$^{-2}$ for the 40 period MQWs and the 25 period MQWs, respectively, were obtained by dividing each 3D carrier density (estimated through the *C-V* profiles) by the number of QWs per unit length. The $E_F(T)$ dependence was evaluated both in the general and nondegenerate cases. For the higher $p_s$ value, the results are given in Fig. 9, where it is shown that the Boltzmann approximation is well justified for the two-dimensional hole gas in the present samples. For comparison, the $E_F(T)$ dependence calculated by Eq. (A3) is also shown in the figure: It can be seen that, as a consequence of neglecting the higher hole subbands, the Fermi level is considerably lowered, although the temperature dependence is not heavily affected.

*Present address: Laboratorio Nazionale MDM, Via C. Olivetti, 2, 20041 Agrate Brianza (MI), Italy.


[1] See, e.g., M. Razeghi, III-Vs Review **10**, 36 (1997).

[2] H. Yi, J. Diaz, B. Lane, and M. Razeghi, Appl. Phys. Lett. **69**, 2983 (1996).

[3] L. J. Mawst, A. Battacharya, J. Lopez, D. Botez, D. Z. Garbuzov, L. DeMarco, J. C. Connolly, M. Jasen, F. Fang, and R. F. Nabiev, Appl. Phys. Lett. **69**, 1532 (1996).

[4]E. Greger, P. Riel, M. Moser, T. Kippenberg, P. Kiesel, and G. H. Döhler, Appl. Phys. Lett. **71**, 3245 (1997).
[5]T. Takamoto, T. Agui, F. Ikeda, and H. Kurita, Sol. Energy Mater. Sol. Cells **66**, 511 (2001).
[6]A. W. Bett, R. Adelhelm, C. Agert, R. Beckert, F. Dimroth, and U. Schubert, Sol. Energy Mater. Sol. Cells **66**, 541 (2001).
[7]N. H. Karam, R. R. King, M. Haddad, J. H. Ermer, H. Yoon, H. L. Cotal, R. Sudharsanan, J. W. Eldredge, K. Edmondson, D. E. Joslin, D. D. Krut, M. Takabashi, W. Nishikawa, M. Gillanders, J. Granata, P. Hebert, B. T. Cavicchi, and D. R. Lillington, Sol. Energy Mater. Sol. Cells **66**, 453 (2001).
[8]E. Gombia, R. Mosca, D. Pal, S. Busi, L. Tarricone, P. G. Fuochi, and M. Lavalle, Mater. Sci. Eng., B **97**, 39 (2003).
[9]R. Magnanini, L. Tarricone, A. Parisini, M. Longo, and E. Gombia, Thin Solid Films (to be published).
[10]Y. J. Chan, D. Pavlidis, M. Razeghi, and F. Omnes, Inst. Phys. Conf. Ser. **106**, 619 (1989).
[11]M. Razeghi, F. Omnes, M. Defour, P. Maurel, P. Bove, Y. J. Chen, and D. Pavlidis, Semicond. Sci. Technol. **5**, 274 (1990).
[12]C. C. Hsu, Y. F. Yang, H. J. Ou, E. S. Yang, and H. B. Lo, Appl. Phys. Lett. **71**, 3248 (1997).
[13]M. A. di Forte-Poisson, C. Brylinski, S. L. Delage, H. Blanck, D. Floriot, S. Cassette, E. Chartier, D. Pons, and A. Huber, Mater. Sci. Eng., B **28**, 242 (1994).
[14]M. Feng, N. Holonyak, Jr., and R. Chen, Appl. Phys. Lett. **87**, 131103 (2005).
[15]Jianhui Chen, J. R. Sites, I. L. Spain, M. J. Hafik, and G. Y. Robinson, Appl. Phys. Lett. **58**, 744 (1991).
[16]G. Arnaud, P. Boring, B. Gil, J. C. Garcia, J. P. Landesman, and M. Leroux, Phys. Rev. B **46**, 1886 (1992).
[17]M. Leroux, M. L. Fille, B. Gil, J. P. Landesman, and J. C. Garcia, Phys. Rev. B **47**, 6465 (1993).
[18]A. Lindell, M. Pessa, A. Salokatve, F. Bernardini, R. M. Nieminen, and M. Paalanen, J. Appl. Phys. **82**, 3374 (1997).
[19]O. Dehaese, X. Wallant, O. Schuler, and F. Mollot, J. Appl. Phys. **84**, 2127 (1998).
[20]J. Martinez-Pastor, J. Camacho, C. Rudamas, A. Cantarero, L. Gonzalez, and K. Syassen, Phys. Status Solidi A **178**, 571 (2000).
[21]S. Froyen, A. Zunger, and A. Mascarenhas, Appl. Phys. Lett. **68**, 2852 (1996).
[22]D. Biswas, N. Debbar, P. Battacharya, M. Razeghi, N. Defour, and F. Omnes, Appl. Phys. Lett. **56**, 833 (1990).
[23]M. A. Rao, E. J. Caine, H. Kroemer, S. I. Long, and D. I. Babic, J. Appl. Phys. **61**, 643 (1987).
[24]M. O. Watanabe and Y. Ohba, Appl. Phys. Lett. **50**, 906 (1987).
[25]M. A. Haase, M. J. Hafich, and G. Y. Robinson, Appl. Phys. Lett. **58**, 616 (1991).
[26]T. Kobayashi, K. Taira, F. Nakamura, and H. Kawai, J. Appl. Phys. **65**, 4898 (1989).
[27]T. W. Lee, P. A. Houston, R. Kumar, X. F. Yang, G. Hill, M. Hopkinson, and P. A. Claxton, Appl. Phys. Lett. **60**, 474 (1992).
[28]Y. Dong, R. M. Feenstra, M. P. Semtsiv, and W. T. Massenlik, Appl. Phys. Lett. **84**, 227 (2004).
[29]S. H. Park, M. Markarian, P. K. L. Yu, and P. M. Asbeck, J. Electron. Mater. **24**, 1381 (1995).
[30]M. S. Faleh, J. Taselli, J. P. Bailbe, and A. Marty, Appl. Phys. Lett. **69**, 1288 (1996).
[31]Y. J. Chan, D. Pavlidis, M. Razeghi, and F. Omnes, IEEE Trans. Electron Devices **37**, 2141 (1990).
[32]See, e.g., A. Zunger and S. Mahajan, in *Handbook on Semiconductors*, edited by T. S. Moss (Elsevier Science, Amsterdam, 1994), Vol. 3, p. 1399; F. Scholz, A. Hangleiter, H. Schweizer, and M. Pilkuhn, III-Vs Review **10**, 38 (1997).
[33]D. V. Lang, M. B. Panish, F. Capasso, J. Allam, R. A. Hamm, A. M. Sergent, and W. T. Tsang, Appl. Phys. Lett. **50**, 736 (1987).
[34]R. E. Cavicchi, D. V. Lang, D. Gershoni, A. M. Sergent, J. M. Vandenberg, S. N. G. Chu, and M. Panish, Appl. Phys. Lett. **54**, 739 (1989).
[35]X. Letartre, D. Stievenard, M. Lannoo, and D. Lippens, J. Appl. Phys. **68**, 116 (1990).
[36]M. Begotti, M. Longo, R. Magnanimi, A. Parisini, L. Tarricone, C. Bocchi, F. Germini, L. Lazzarini, L. Nasi, and M. Geddo, Appl. Surf. Sci. **222**, 423 (2004).
[37]M. Longo, R. Magnanini, A. Parisini, L. Tarricone, C. Bocchi, F. Germini, L. Lazzarini, and L. Nasi, Extended Abstracts of the 12th European Workshop on Metalorganic Vapour Phase Epitaxy, Bratislava, Slovakia, 2007, G1, pp.239–242.
[38]M. Longo, R. Magnanini, A. Parisini, L. Tarricone, A. Carbognani, C. Bocchi, and E. Gombia, J. Cryst. Growth **248**, 119 (2003).
[39]C. Ghezzi, M. Longo, R. Magnanini, A. Parisini, L. Tarricone, A. Carbognani, C. Bocchi, and E. Gombia, Phys. Status Solidi C **0**, 835 (2003).
[40]See, e.g.. C. R. Moon, Byung-Doo Choe, S. D. Kwan, and H. Lim, Appl. Phys. Lett. **70**, 2987 (1997).
[41]E. Gombia, C. Ghezzi, A. Parisini, L. Tarricone, and M. Longo, Mater. Sci. Eng., B **147**, 171 (2008).
[42]M. Longo, A. Parisini, L. Tarricone, L. Toni, and R. Kudela, Mater. Sci. Eng., B **86**, 157 (2001).
[43]J. Martinez-Pastor, L. Gonzales, and P. Roussignol, Appl. Phys. Lett. **68**, 2111 (1996).
[44]J. P. Landesman, J. C. Garcia, J. Massies, P. Maurel, G. Jezequel, J. P. Hirtz, and P. Alnot, Appl. Phys. Lett. **60**, 1241 (1992).
[45]X. B., Zhang, J. H. Ryou, R. D. Dupuis, G. Walter, and N., Holonyak, Jr., J. Electron. Mater. **35**, 705 (2006).
[46]T. Nakano, Y. Nakano, and Y. Shimogaki, J. Cryst. Growth **221**, 136 (2000).
[47]H. Sai, H. Fujikura, A. Hirama, and H. Hasegawa, Solid-State Electron. **43**, 1541 (1999).
[48]W. Stolz and T. Whithaker, Compound Semicond. **5**, 29 (1999).
[49]S. H. Lee and B. Stringfellow, J. Appl. Phys. **83**, 3620 (1998).